PROCEEDINGS OF SCIENCE

Subluminal Pulses in the Surface-Scintillator Detectors of AugerPrime

Tobias Schulz[a,b,*] **for the Pierre Auger Collaboration**[c]

[a] *Institute for Astroparticle Physics, Karlsruhe Institute of Technology (KIT)*
Karlsruhe, Germany

[b] *Instituto de Tecnologías en Detección y Astropartículas (CNEA, CONICET, UNSAM)*
Buenos Aires, Argentina

[c] *Full author list:* https://www.auger.org/archive/authors_2024_11.html

E-mail: spokespersons@auger.org

In extensive air showers, the signals from the electromagnetic and muonic components typically span a few microseconds in scintillation detectors. Neutrons are the only stable neutral hadrons over the timescale of air showers. They lose energy exclusively through hadronic interactions and quasi-elastic scattering, which results in their high abundance at ground level. These neutrons can produce delayed pulses in scintillation detectors, appearing up to several milliseconds after the primary shower signal. This allows us to probe hadronic interactions in the development of air showers. In this study, we characterize such subluminal pulses using the first measurements from the scintillator surface detectors of the AugerPrime upgrade of the Pierre Auger Observatory.

7th International Symposium on Ultra High Energy Cosmic Rays (UHECR2024)
17-21 November 2024
Malargüe, Mendoza, Argentina

*Speaker

 ISSN 1824-8039 . Published by SISSA Medialab.

PoS(UHECR2024)050

1. Introduction

The measurement of extensive air showers and the separation of their components are important for testing hadronic interaction models at ultra-high energies. They must be extrapolated for the simulation of air showers because the primary cosmic rays can exceed the energies achievable by human-made accelerators by several orders of magnitude. An air shower can be divided into electromagnetic and hadronic shower components. From the hadronic shower component, neutrons are the only relevant massive and neutral particles that are stable long enough to reach the ground. Simulations of extensive air showers have shown that neutrons with a broad energy spectrum can reach the ground with possible delays of up to several seconds following the initial shower front [1, 2]. Pulses with such large delays were measured and documented in 1984 by John Linsley with the scintillator detectors of the Volcano Ranch experiment [3]. He assumed these pulses could correspond to neutrons traveling at speeds slightly below the speed of light, an idea previously suggested by Kenneth Greisen [5]. Since neutrons are neutral particles, therefore they can produce a signal in a scintillator only through elastic and inelastic scattering with nuclei in the scintillator material or via neutron capture processes that emit gamma rays. In the upgrade of the Pierre Auger Observatory [4] known as *AugerPrime* [6], *Surface-Scintillator detectors* (SSDs) were installed atop the existing *Water-Cherenkov detectors* (WCDs). During early SSD measurements with the pre-production array, delayed pulses were observed in the time traces [7].

2. Data collection and candidate selection

The optimal efficiency of the SSD in detecting neutron pulses is expected to begin at energies around a few MeV. Below 0.7 MeV, the probability of detecting a neutron in the scintillator drops below 0.001%. Conversely, at energies above 100 MeV, the efficiency in detecting neutrons reaches approximately 2.3% [2]. The available data from the AugerPrime upgrade are used for this analysis, comprising measurements from 2020 through 2024. The minimal reconstructed shower energy is set to 10^{18} eV and the zenith angles of the showers are limited to a maximum of 60°. This selection yields a dataset of 199 973 events with 613 794 time traces. Only traces from the high-gain channel of the SSD photomultiplier tube (PMT), which are free from baseline saturation caused by undershoot, are included in the analysis. The peak and integral of a signal produced by a vertical minimal ionizing particle are defined as $\mathrm{MIP_{peak}}$ and $\mathrm{MIP_{charge}}$, respectively. A simple pulse-finding algorithm is applied to each trace. A typical pulse charge from a single photoelectron is approximately $0.05\,\mathrm{MIP_{charge}}$. The pulse start time $t^{\mathrm{start}}_{\mathrm{pulse}}$ is defined as the moment when a bin value in the trace exceeds a conservative value of $0.8\,\mathrm{MIP_{peak}}$. The pulse end time is determined when the bin value drops below $0.8\,\mathrm{MIP_{peak}}$ for two consecutive bins to mitigate the effects of afterpulsing or electronic noise. The pulse start and end times are measured relative to the signal start time t_{start}, determined by the WCD. The charge S_{pulse} for each pulse is obtained by integrating the signal from the start to the stop bin, expressed in units of $\mathrm{MIP_{charge}}$. If a pulse is sufficiently large to saturate the trace, the low-gain channel is used instead to estimate S_{pulse}.

In Fig. 1 an example time trace of the SSD with visible late pulses is shown. At $t^{\mathrm{start}}_{\mathrm{pulse}} = 0$, the passage of the shower front generates a broad signal. Pulses that arrive before this would likely be caused by atmospheric muons. The majority of pulses occur within approximately 2.5 µs. These

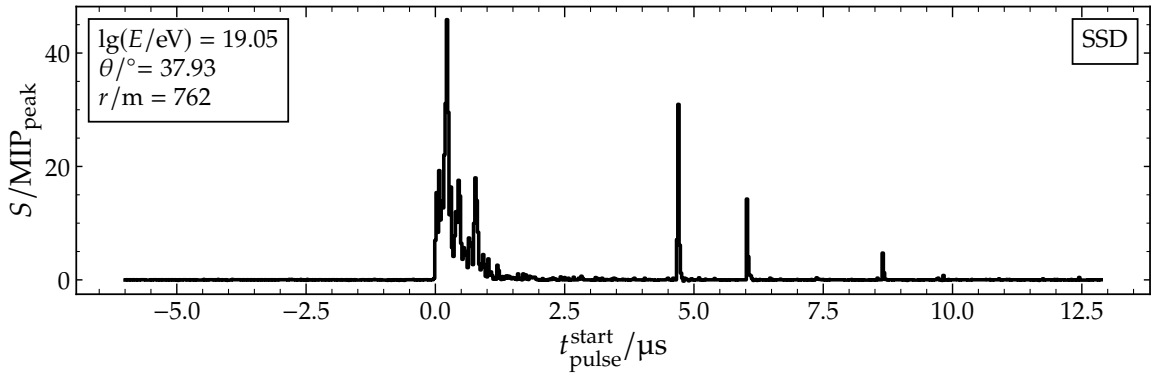

Figure 1: An example SSD trace is shown for a station participating in an event of the pre-production array. The time $t_{\text{pulse}}^{\text{start}}$ is adjusted to commence at the estimated start of the passage of the shower front. Three large, late pulses are notable in the SSD trace.

late pulses can reach charges up to 220 $\text{MIP}_{\text{charge}}$ with an average duration of around 0.03 µs. A time threshold of $t_{\text{pulse}}^{\text{start}} \geq 5$ µs is set to select candidate pulses that may originate from delayed neutrons. This threshold is chosen to be sufficiently long after the initial shower front to resolve individual pulses. Additionally, the background contribution from other particles of electromagnetic or muonic origin is quantified using air shower simulations. 60 000 showers are simulated, using the CORSIKA simulation software [8]. The events consist of a mixture of 4 primary particles (proton, helium, oxygen, iron) in a 1:1:1:1 ratio. They are distributed uniformly over $\sin^2\theta$, with θ ranging from 0 to 60°, and energy, ranging from 10^{18} eV to $10^{19.5}$ eV. The utilized hadronic interaction model is EPOS-LHC, and the hadron energy cut-off in the simulated showers is set at 20 MeV. The Offline software framework [9] is utilized for the detector simulation and shower reconstruction. In the distance range of 400 to 800 m from the shower axis, for pulses exceeding approximately 11 $\text{MIP}_{\text{charge}}$, the background of non-hadronic pulses is around 3%. This background increases to about 15% for pulses below 11 $\text{MIP}_{\text{charge}}$. Depending on the shower energy, zenith angle, distance to the shower axis, and the charge of the individual pulses, the fraction of pulses arising from muonic and electromagnetic particles past 5 µs ranges between around 1 and 30%.

3. Measurement of subluminal pulse rate

In Fig. 2-left, the average number of candidate pulses N_{pulses} per trace as a function of distance from the shower axis is shown for events 1.0 and 1.2 in sec θ. In the energy range from $10^{18.5}$ eV to 10^{19} eV and at a distance of 1000 m from the shower axis, a total of 1310 late pulses are detected across 7268 traces, resulting in an expected pulse rate of approximately 18 % per trace. At a closer distance of around 600 m, this rate increases to 43 % with 1049 late pulses observed in 2439 traces. In the lower energy range from 10^{18} eV to $10^{18.5}$ eV at 1000 m from the shower axis, 5189 late pulses are recorded in a total of 84 676 traces, yielding a pulse rate of 9 %. Similarly, at 600 m, the pulse rate rises to 13 % with 3769 late pulses detected in 28 656 traces. All pulses arriving at $t_{\text{pulse}}^{\text{start}} < -0.2$ µs are classified as background pulses unrelated to the shower. Their rate is calculated and then normalized to the counting window of the late pulses. At the closest distances to the shower axis, the late pulse rate surpasses the background pulse rate by over two orders of magnitude. As

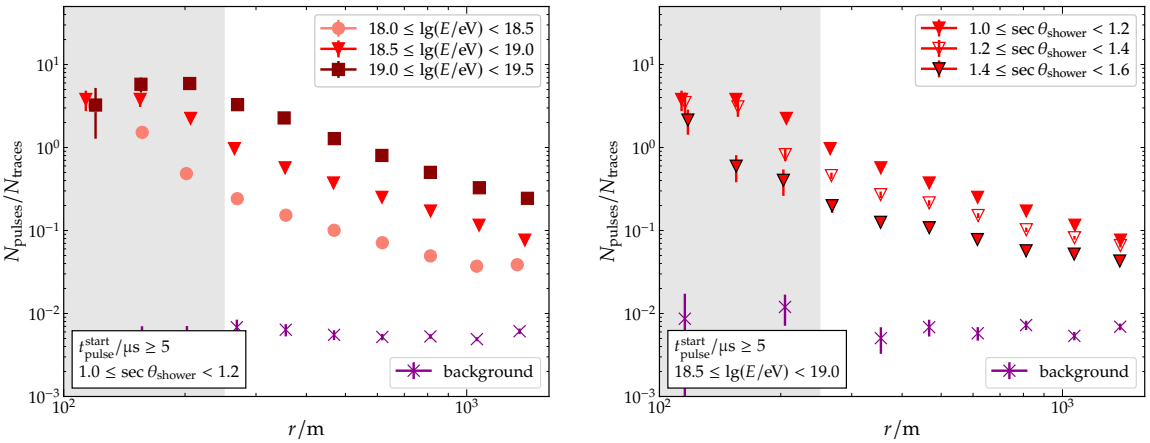

Figure 2: *Left:* The average amount of candidate pulses N_{pulses} per trace increases with energy and decreases with distance to the shower axis. Below around 250 m from the shower axis (shaded area), the rate begins to plateau due to increasing saturation of the electronics baseline due to undershoot. *Right:* With increasing sec θ the pulse rate decreases.

previously mentioned, the pulse rates include pulses from a potential hadronic component. They are contaminated with pulses from muonic or electromagnetic components, which are not accounted for in the background estimation. This additional background varies with the zenith angle, shower energy, and pulse signal. In Fig. 2-right, the pulse rate is shown for a fixed energy range from $10^{18.5}$ eV to 10^{19} eV across different bins in sec θ. The pulse rate decreases with increasing sec θ of the shower. The rate begins to plateau at distances below 250 m from the shower axis. This behavior can be attributed to the saturation of the electronics baseline due to undershoot. The fraction of stations with a saturated baseline $N_{\text{sat}}/N_{\text{tot}}$ rapidly increases, starting at approximately 250 m from the shower axis. Since pulses cannot be reliably counted in traces with a saturated baseline caused by undershoot, a reduced counting rate in this region is expected.

4. Measurement of subluminal pulse amplitude spectrum

The individual charges, S_{pulse}, of all candidate pulses measured are combined to obtain a pulse amplitude spectrum are shown. To compare the shapes of different pulse spectra - categorized into bins based on energy, shower zenith angle, and distance - the number of pulses N_{pulse} in each bin is normalized to the total number of pulses N_{tot} within the corresponding signal bin. No apparent dependence of the pulse spectrum shape on varying shower energies or zenith angles is observed. Consequently, the energy and zenith angle bins are combined to improve statistical significance. In Fig. 3-left, the pulse amplitude spectra for three distance bins, ranging between 0 and 400, 400 and 800, and 800 and 2000 m from the shower axis are shown. As the distance from the shower axis increases, the spectrum softens, and a noticeable cut-off of pulses above approximately 10 $\text{MIP}_{\text{charge}}$ appears.

In Ref. [2], the FLUKA simulation framework [10, 11] was used to demonstrate that the shape of the neutron energy spectrum varies depending on both the arrival time relative to the shower signal and the distance from the shower axis. In Fig. 3-right simulated neutron spectra from Ref.

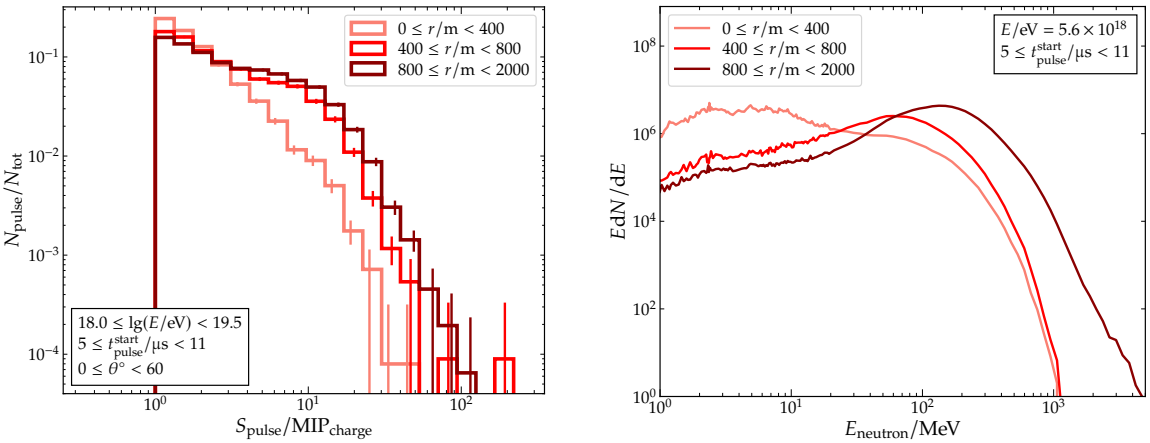

Figure 3: *Left:* The measured pulse spectrum for three distance bins. With increasing distance to the shower axis, a hardening of the spectrum can be observed. *Right:* Three simulated neutron spectra of Ref. [2], with a comparable parameter space as for the measurements. In the observed time range between 5 and 11 µs, the energy spectrum of neutrons extends to larger energies.

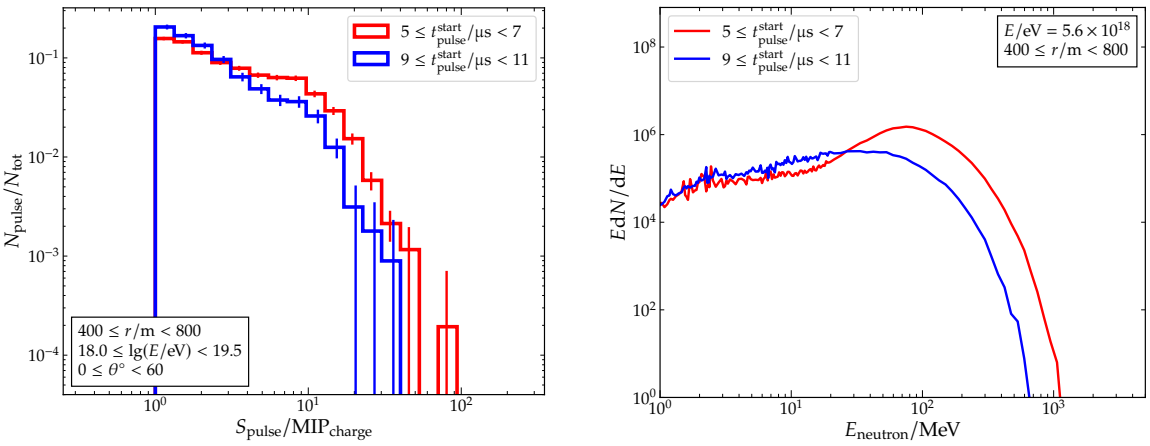

Figure 4: *Left:* When binning the pulse spectrum for different pulse arrival times, the spectrum, containing earlier (5 and 7 µs) pulses, reaches to larger S_{pulse} than when considering later (9 and 11 µs) pulses. This trend corresponds to the expectation that neutrons arriving earlier on the ground have larger energies than neutrons arriving later. *Right:* Two simulated neutron spectra of Ref. [2], with a comparable parameter space as for the measurements.

[2] at a shower energy of 5.6×10^{18} eV across three distinct distance bins, corresponding to those used in the measurements, are shown. Within the chosen time window of 5 to 11 µs, the energy spectrum extends to higher energies as the distance from the shower axis increases.

The pulse amplitude spectrum for the distance bin between 400 and 800 m gets separated between 'early' and 'late' pulse arrival times. Early arrival times are defined between 5 and 7 µs, while late arrival times are between 9 and 11 µs. In Fig. 4-left, the pulse amplitude spectra for these two arrival time bins are displayed, showing a slight hardening of the spectrum for the early arrival times. In Fig. 4-right, two simulated neutron spectra of Ref. [2] are shown for a shower energy of 5.6×10^{18} eV and a distance from 400 to 800 m to the shower axis and the same arrival time bins

as used in the measurements. The simulated spectra exhibit similar behavior to the neutron energy spectra, with neutrons at early arrival times extending to larger energies.

5. Forward-folding neutron energy spectra

A preliminary simulation of possible pulse amplitude spectra from neutrons in the SSD is performed. To achieve this, single neutrons with fixed energies E_{neutron} are injected into the SSD using the $\overline{\text{Off}}\underline{\text{line}}$ framework. The energies range from 1 MeV to 4700 MeV and are divided into 54 logarithmic bins. For each energy bin 500 000 neutrons are simulated at an average angle of 45°. Additionally, Birks' law is applied to account for quenching effects in the scintillator, using a constant of ≈ 0.126 mm/MeV for polystyrene-based scintillators [12] as a first approximation. The resulting neutron pulses, S_{pulse}, in the SSD are then analyzed using the same pulse-finding algorithm used for the neutron measurements. The input energy spectra follow power-laws, where $\mathrm{d}N/\mathrm{d}E \propto E^1$ and $\mathrm{d}N/\mathrm{d}E \propto E^{-1}$. Furthermore, an input energy spectrum from Ref. [2] is utilized, involving neutrons in a vertical shower with an energy of 5.6×10^{18} eV at an atmospheric depth of about 878 g/cm^2, corresponding to the same depth as in the measurements. This spectrum includes all downward-going neutrons within a distance range of 400 m to 800 m from the shower axis and arrival times between 5 µs and 11 µs. A scaling factor is determined for each input neutron energy spectrum and corresponding energy bin. Subsequently, the scaled pulse spectra from these simulations are aggregated into the total pulse spectrum. The final total pulse spectrum is then normalized to the total number of pulses, enabling the comparison with the measurements.

The pulse amplitude spectra corresponding to their three input energy spectra are shown in Fig. 5. Each neutron energy contribution is color-coded to visualize its relative impact on the full spectrum. These three plots demonstrate a strong dependence of the pulse amplitude spectrum on the shape of the input energy spectrum. The forward-folded pulse amplitude spectrum could be further enhanced by using a more complex angular distribution of neutrons rather than a single average angle and by obtaining a more precise estimation of the quenching constant.

6. Conclusions

Late pulses are observed in measurements from the new AugerPrime SSD dataset, revealing rates up to three orders of magnitude higher than the expected background pulses. Simulations of air showers indicate that the fraction of pulses originating from muonic and electromagnetic components ranges from 1% to 30%, depending on the primary energy, zenith angle, and distance from the shower axis. Additionally, the signal spectrum of the late pulses was examined, and its shape appears to be largely independent of both primary energy and zenith angle. However, a hardening of the spectrum is observed with increasing distances from the shower axis. This hardening could arise from the limitation of the time window in the traces, within which the delayed pulses are counted. Using the $\overline{\text{Off}}\underline{\text{line}}$ simulation framework, pulse amplitude spectra from the SSD signal responses for neutrons at different energies and impact angles were generated. By forward-folding arbitrary neutron energy spectra using the signal responses, it is demonstrated how the pulse amplitude spectrum depends on the shape of the neutron energy spectrum and that AugerPrime is sensitive to the shape. A comparison between the SSD measurements and FLUKA simulations of

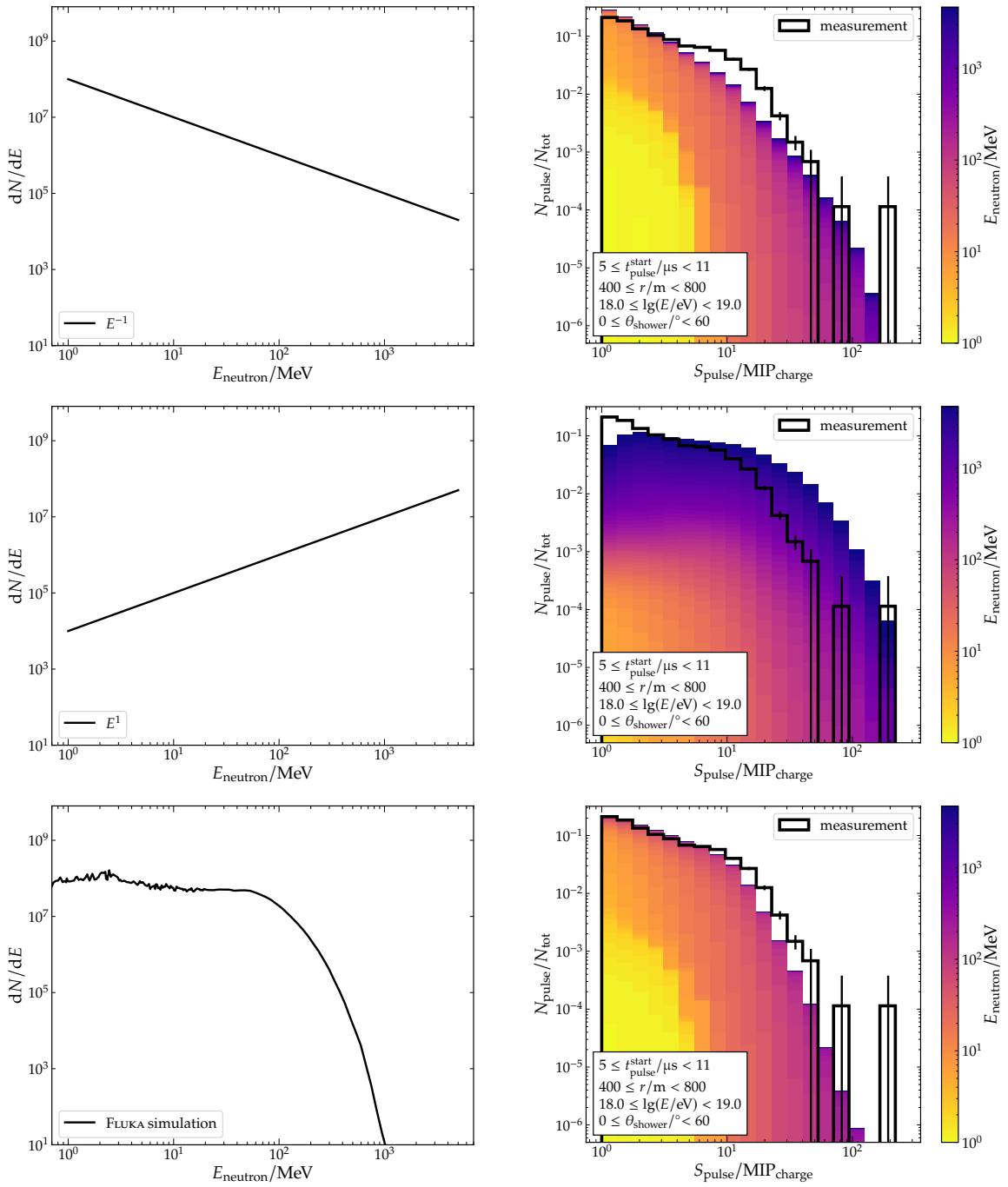

Figure 5: The simulated pulse amplitudes are sampled from different input energy spectra (left plots). The resulting pulse amplitude spectra (right plots) can then be compared with the measured pulse spectrum. The contribution of each neutron energy is color-coded to visualize its relative contribution to the full spectrum.

a neutron energy spectrum from Ref. [2] showed first-order agreement. The measurement of late pulses in the SSD of the AugerPrime upgrade suggests that the neutron component of air showers can be further studied at the Pierre Auger Observatory. While the rate of late pulses is likely too low to permit event-by-event analysis at primary energies below $10^{19.5}$ eV, the cumulative data from the expanding Phase II dataset can be used for further studies and to compare predictions from various hadronic interaction models regarding the neutron content of air showers.

References

[1] A. D. Erlykin, Nucl. Phys. B Proc. Suppl. **175-176** (2008), 330-333.
[2] M. Schimassek *et al.*, arXiv:2406.11702.
[3] J. Linsley, J. Phys. G **10** (1984), L191-L195.
[4] A. Aab *et al.* [Pierre Auger], Nucl. Instrum. Meth. A **798** (2015), 172-213.
[5] K. Greisen, Proc. **5th Interamerican Seminar on Cosmic Rays** (1962), Vol.2, XLVII-2
[6] A. Aab *et al.* [Pierre Auger], arXiv:1604.03637.
[7] P. Abreu *et al.* [Pierre Auger], PoS **ICRC2021** (2021), 218.
[8] D. Heck *et al.*, FZKA **6019** (1998).
[9] S. Argiro *et al.*, Nucl. Instrum. Meth. A **580** (2007), 1485-1496.
[10] A. Ferrari *et al.*, doi:10.2172/877507.
[11] T. T. Böhlen *et al.*, Nucl. Data Sheets **120** (2014) 211-214.
[12] R. L. Workman *et al.* [Particle Data Group], PTEP **2022** (2022) 083C01.